Electron Shuttle between Membrane-Bound Cytochrome P450 3A4 and b_5 Rules Uncoupling Mechanisms†

Alain Perret and Denis Pompon*

Laboratoire d'Ingénierie des Protéines Membranaires, Centre de Génétique Moléculaire du CNRS, F91198 Gif-sur-Yvette Cedex, France

Received April 21, 1998; Revised Manuscript Received June 3, 1998

ABSTRACT: Contradictory mechanisms involving conformational or redox effects have been proposed for the enhancement of cytochrome P450 activities by cytochrome b_5 in reconstituted systems. These mechanisms were reinvestigated for human liver P450 3A4 bound to recombinant yeast membranes including human P450 reductase and various levels of human b_5. Species conversions were calculated on the basis of substrate, oxygen, and electronic balances in six different substrate conditions. Electron flow from P450 reductase to ferric 3A4 was highly dependent on the nature of substrate but not on the presence of b_5. P450 uncoupling by hydrogen peroxide formation was decreased by b_5, leading to a corresponding increase in the rate of ferryl−oxo complex formation. Nevertheless, the major b_5 effects mainly relied on an increased partition of ferryl−oxo complex to substrate oxidation compared to reduction to water, which could support a conformation change based mechanism. However, further steady-state investigations evidenced that electron carrier properties of b_5 were strictly required for this modulation and that redox state of b_5 was ruled by the nature and concentration of 3A4 substrates. Moreover, rapid kinetic analysis of b_5 reduction following NADPH addition suggested that b_5 was reduced by the 3A4 ferrous−dioxygen complex and reoxidized by subsequent P450 oxygenated intermediates. A kinetic model involving a 3A4−b_5 electron shuttle within a single productive P450 cycle was designed and adjusted. This model semiquantitatively simulated all presented experimental data and can be made compatible with the effect of the redox-inactive b_5 analogue previously reported in reconstituted systems. In this model, synchronization of the b_5 and 3A4 redox cycles, binding site overlap between b_5 and reductase, and dynamics of the b_5−3A4 complex were critical features. This model opened the way for designing complementary experiments for unification of b_5 action mechanisms on P450s.

In mammals, cytochrome P450s (P450)[1] are membrane-bound heme−thiolate proteins involved in the oxidative metabolism of xenobiotic and endobiotic compounds (*1*−*3*). P450s are not self-sufficient enzymes, and microsomal forms require NADPH−cytochrome P450 reductase (CPR) as electron carrier for function. In human liver, CYP3A4 (3A4) is a major P450 isoenzyme that plays a critical role in the metabolism of natural xenobiotics and many clinically important drugs (*4*). Activities of purified 3A4 in artificial reconstituted systems including CPR were found highly dependent on lipid nature (*5*−*9*), salt composition (*8, 10, 11*), and presence of detergents (*5*−*8, 12*) and additive agents (*11, 13*). Cytochrome b_5 (b_5), an electron carrier involved in fatty acid biosynthesis (*14*), was early found to modulate microsomal P450 activity in a way highly dependent on P450 isoenzyme, nature of substrate (*15, 16*), and CPR origin and concentration (*17, 18*). Addition of b_5 to P450-containing reconstituted systems could have no effect, inhibit, or strongly enhance P450 activities depending on experimental conditions (*19*). Enhancing effects of b_5 have been mainly studied in reconstituted systems involving a high CPR to P450 molar ratio (frequently 3:1) irrespective of the low ratio (about 1:10) found in liver. A role for b_5 was proposed to be an alternate electron donor for reduction of the P450 ferrous−dioxygen complex, thus promoting active oxygen (ferryl−oxo P450) formation (*20*−*24*). Reduction of the $P450_{LM2}$ ferrous−dioxygen complex by b_5 was confirmed by rapid mixing experiments (*25, 26*). Loss of b_5 effects upon reconstitution with redox-inactive heme analogues also supported this finding (*16, 27*−*29*). However, contrasting results were obtained with rabbit $P450_{LM4}$ (*26*). Furthermore, a high-spin shift and an increased substrate affinity of $P450_{LM2}$ or $P450_{RLM5}$ upon b_5 binding indicated that b_5 could alter P450 conformation (*23, 25, 30*), suggesting that electron transfers may only partly explain the b_5 effects. Reports that binding of manganese- and iron- (native) b_5 to $P450_{LM2}$ and $P450_{LM4}$ caused similar decrease in the K_m for benzphetamine and acetanilide oxidation (*28*) and that heme-free b_5 could be, in reconstituted systems, as effective as native b_5 in enhancing 3A4 activities (*31*) confirmed this finding. Therefore, b_5 effects could involve both conformational and redox

† This work was supported by Grant 6242 from the Association pour la Recherche sur le Cancer. Financial support for A.P. was given by Fellowship FC 30130 from the Fondation pour la Recherche Médicale.

* To whom correspondence should be addressed: Centre de Génétique Moléculaire du CNRS, UPR 9061, Avenue de la Terrasse, 91198 Gif-sur-Yvette Cedex, France. Tel: (+33) 169823181. Fax: (+33) 169075539. E-mail: pompon@cgm.cnrs-gif.fr.

[1] Abbreviations: P450, cytochrome P450; CPR, NADPH−cytochrome P450 reductase; 3A4, cytochrome P450 3A4; b_5, cytochrome b_5; PMSF, phenylmethanesulfonyl fluoride; TFA, trifluoroacetic acid.

S0006-2960(98)00908-8 CCC: $15.00
Published on Web 07/31/1998

contributions, and the dominant effect could be isoenzyme dependent. Nevertheless, these reported contradictory effects questioned if the variability of observations might also relate to the use of different experimental systems leading to different limiting steps in the mechanism. Recent development of high-efficiency recombinant expression systems opened the way to the analysis of the b_5−P450−CPR coupling mechanisms in a natural membrane environment (*32*−*34*). Particularly, membranes containing high CPR to P450 molar ratios (up to 10:1) were produced using baculovirus expression systems (*35*−*37*). More physiological conditions can be achieved using the yeast expression system which allowed expression of human 3A4 at a high level while achieving the low (1:10) CPR to P450 molar ratio representative of the liver situation (*38*−*41*). In the yeast system, interfering endogenous activities can be removed by gene disruption (*18, 42*), and tunable levels of b_5 can be achieved by self-incorporation of purified recombinant human b_5 in membranes.

Most of microsomal P450s are poorly coupled enzymes producing large amounts of hydrogen peroxide and uncoupled water by four-electron reduction of dioxygen. Hydrogen peroxide formation occurs either by decomposition of the ferrous−dioxygen complex or by direct release from the peroxy−ferric intermediate (*43, 44*). Water formation exceeding the product-forming reaction occurs via a bielectronic reduction of the ferryl−oxo complex (*45*−*47*). These abortive reactions are controlled by electron transfers within the P450−CPR−b_5 complexes and by the stability of oxygenated intermediates, making these phenomena highly dependent on P450 environment. We report here a detailed analysis by steady-state, rapid kinetic, and numerical simulation of 3A4 uncoupling control by b_5 in natural membranes. The work evidenced critical roles of electron shuttles between 3A4 and b_5 and of the structure and dynamic of the reductase−3A4−b_5 complexes.

EXPERIMENTAL PROCEDURES

Chemicals. NADPH, testosterone, androstenedione, nifedipine, quinidine, homovanillic acid, cinnamic acid, α-naphthoflavone, phenacetin, and phenylmethanesulfonyl fluoride (PMSF) were purchased from Sigma. Cobalt sepulchrate trichloride was purchased from Aldrich. Testosterone and androstenedione metabolites were purchased from Steraloids. Cyclosporin A and its M1 and M17 metabolites were a gift from Sandoz. The nifedipine metabolite was synthesized according to Loev and Snader (*48*). The *N*-oxide metabolite of quinidine was a gift from Pr. Philippe Beaune. Trifluoroacetic acid (TFA) was from Fluka. DEAE columns were from Pharmacia, and hydroxylapatite columns were from Calbiochem-Novabiochem. Octadecylsilyl Newguards (7 μm particle size, 15 mm × 3.2 mm) and Spheri-5 columns (5 μm particle size, 100−2.1 mm) were from Brownlee.

Enzymes. Lysozyme, DNase, RNase, and horseradish peroxidase were purchased from Sigma. Restrictions enzymes were purchased from New England Biolabs.

Yeast Strains and Plasmids. Yeast strain W(hR) which was genetically engineered to express human CPR instead of the yeast enzyme, has been described previously (*17, 18*). The expression vectors for 3A4 and yeast transformation were described earlier (*49*). Cell cultures were grown and microsomes prepared as previously described (*50*) except that the PEG membrane precipitation step was omitted and substituted by ultracentrifugation at 100000*g* for 1 h at 4 °C. The pellet of microsomes was resuspended in a minimal volume of 3 mL of 50 mM Tris-HCl, pH 7.4, and kept frozen at −80 °C for months. Total P450 content was calculated from the reduced carbon monoxide difference spectrum using a Perkin-Elmer Lambda 2 spectrophotometer and was close to 1000 pmol/mg of microsomal proteins. NADPH−cytochrome *c* reductase activities were measured as previously published (*51*). Protein concentration was determined using the Pierce bicinchoninic acid procedure.

b_5 Expression and Purification. The open reading frame of human b_5 cloned in pUHE21 (gift from Dr. Philippe Urban) was used to transform the BMH 71-18 *Escherichia coli* strain. A single colony was grown in Terrific Browth medium containing 100 μg/mL ampicillin for 72 h with shaking at 22 °C. Cells were harvested by centrifugation at 4000*g*, and the resulting pellet was resuspended and incubated for 30 min in 50 mM Tris-HCl, pH 7.4, containing 1 mM PMSF and 1 mg/mL lysozyme. Cells were lysed by sonication. Then 0.02 mg/mL RNase and 0.05 mg/mL DNase were added, and b_5 was solubilized at 4 °C with 1% (w/v) sodium cholate, pH 7.4, for 1 h with moderate shaking. Supernatant was loaded onto a DEAE-cellulose anion-exchange column equilibrated with 0.2% (w/v) sodium cholate, 20 mM sodium/potassium phosphate buffer, pH 7.4. b_5 was eluted with 0.5 M NaCl, 0.2% cholate, and 20 mM sodium/potassium phosphate buffer, pH 7.4. Fractions containing b_5 were applied to a hydroxylapatite column equilibrated with 0.5 M NaCl and 20 mM sodium/potassium phosphate buffer, pH 7.4. Pure b_5 was eluted with 0.1% (w/v) sodium cholate and 0.5 M sodium/potassium phosphate buffer and dialyzed against 0.1% (w/v) sodium cholate, 1 mM PMSF, and 20 mM sodium/potassium phosphate buffer. b_5 was concentrated and stored at −20 °C for months.

Preparation of b_5 Analogues. Apo-b_5 was prepared by a modification of the procedure of Strittmatter (*52*). Briefly, 1 mL of 40 μM native b_5 (Fe-b_5) was rapidly mixed at 0 °C with 10 mL of acid acetone [containing 0.2% (v/v) concentrated HCl]. The temperature was immediately decreased to −40 °C in dry ice−acetone, and the suspension centrifuged for 10 min at 10 000 rpm. The pellet was washed at −40 °C with pure acetone and centrifuged again. Residual acetone was evaporated, and the pellet was resuspended in 0.5 mL of 50 mM phosphate buffer, pH 7.4, containing 0.5% (w/v) sodium cholate, pH 7.4, before addition of 1 mL of 6 M guanidinium chloride, giving a clear solution. Two stoichiometries of metal analogue protoporphyrin dissolved in dimethylformamide were added. The mix was 10-fold stepwise diluted by 50 mM phosphate buffer, pH 7.4, at 0 °C and loaded onto a hydroxylapatite column equilibrated with 50 mM phosphate buffer containing 0.5% (w/v) sodium cholate. The reconstituted b_5 analogue was eluted with 0.5 M phosphate buffer containing 0.1% (w/v) sodium cholate and dialyzed against 50 mM phosphate buffer before storage at −20 °C. Zinc(II) protoporphyrin was purchased from Sigma. Cobalt(III) mesoporphyrin was prepared according to Clark et al. (*53*).

P450 3A4 Activities. For activity determinations, P450 3A4 (50 pmol) was incubated for 15 min at 28 °C in 500 μL of standard buffer (5 mM MOPS/NaOH, 200 mM LiCl,

pH 7.0) containing 100 μM NADPH and 200 μM substrate (testosterone, androstenedione, quinidine, and nifedipine) or 70 μM cyclosporin A. Standard buffer was designed to optimize 3A4 activities. Use of NaCl instead of LiCl containing buffer led to comparable results in all reported experiments.

When present, b_5 was added at a b_5:3A4 molar ratio of 2:1 and was left to self-incorporate into membranes for 10 min at 0 °C (incorporation was complete in a few minutes as judged by stabilization of all enzymatic parameters). Reactions were started by addition of NADPH and quenched with 1 μL of TFA except for quinidine reactions which were quenched according to Guengerich et al. (*54*). Extractions were performed with 500 μL of dichloromethane. Organic phases were evaporated under a nitrogen stream, and residues were solubilized in 20 μL of methanol and 180 μL of water for HPLC analysis. Separations were accomplished using a Waters 600 HPLC. Steroids and metabolites were monitored at 254 nm. A linear gradient (6 min, 1.25 mL/min) from 1:10:0.02 to 6:4:0.02 acetonitrile:water:TFA (by volume) was used, followed by an isocratic elution for 2 min. Nifedipine and its metabolite were monitored at 271 nm and eluted with a linear gradient from 22:78:0.2 to 60:40:0.2 acetonitrile: water:TFA over 5 min, followed by an isocratic elution for 2 min. Cyclosporin A and its metabolites were monitored at 205 nm and eluted with a 30 min acetonitrile:water:TFA linear gradient from 30:70:0.2 to 40:60:0.2 and a 10 min linear gradient to 60:40:0.2 followed by a 3 min plateau. Quinidine and its metabolites were monitored using a Jasco fluorescence detector (excitation at 240 nm, emission at 380 nm) and eluted using a 1.25 mL/min linear gradient from 20% to 55% (v/v) acetonitrile in 25 mM triethylamine acetate in water over 14 min, followed by an isocratic elution for 2 min.

NADPH Oxidation. The rate of NADPH oxidation was determined at 28 °C by differential spectroscopy at 340 nm. The assay containing microsomes (120 pmol of P450) in 1.2 mL of standard buffer, 200 μM substrate (testosterone, androstenedione, quinidine, and nifedipine), or 70 μM cyclosporin A was equally divided between sample and reference cuvettes. NADPH (100 μM final) and water were added to the sample and reference cuvettes, respectively. The rate of NADPH oxidation was deduced from the slope of the 340 nm absorbance trace. This rate represents the sum of 3A4-dependent and background NADPH oxidation rates. This background was evaluated from a control experiment in which ketoconazole (25 μM) was added to the assay mixture to fully inhibit P450. Very similar background values were obtained using the same amount of microsomal proteins from control strain lacking 3A4 expression. Corrected values thus represent only the 3A4 contribution to the rate of NADPH oxidation in the membrane fractions.

Hydrogen Peroxide Formation. Measurement of hydrogen peroxide was based on the method of Guilbault et al. (*55*), which involves conversion of nonfluorescent homovanillic acid to its highly fluorescent dimer by hydrogen peroxide in the presence of horseradish peroxidase. Assays were performed in 500 μL of standard buffer containing membranes (50 pmol of 3A4). Reactions were quenched after 0, 1, 2, 3, and 4 min with 1 μL of TFA. Following neutralization, 10 μL of a 25 mg/mL homovanillic acid in water and 1 μg of horseradish peroxidase were added, and the mixture was incubated at room temperature for 5 min. The mixture was acidified with 2.5 μL of TFA. Extraction was performed with 500 μL of NaCl-saturated water and 500 μL of ethyl acetate. Organic extracts were evaporated under a nitrogen stream, and residues were solubilized in 20 μL of methanol and 180 μL of water for quantification by HPLC. The column was first washed for 2 min at 1.25 mL/min with a 1:9:0.02 mix and eluted by a linear gradient to 6:4:0.02 acetonitrile:water:TFA for 2 min. Fluorescent detection of product was performed using excitation at 315 nm and emission at 425 nm. No background above the detection limit was found with membrane devoid of 3A4 or inhibited by ketoconazole. To correct for hydrogen peroxide instability in our 3A4 incubation conditions, the observed time-dependent accumulation of H_2O_2 was fitted according to the integrated form (eq 2) of the differential equation (eq 1) which assumes a constant rate of formation and a pseudo-first-order law of decomposition of the accumulated hydrogen peroxide.

$$\frac{d[H_2O_2]}{dt} = k - k_1[H_2O_2] \quad (1)$$

$$[H_2O_2] = \frac{k}{k_1} - \frac{k \exp(-k_1 t)}{k_1} \quad (2)$$

k and k_1 represent the rate constants for formation and decomposition of hydrogen peroxide, respectively. These rate constants were obtained from optimal fitting of experimental data using eq 2 and nonlinear iterative regression.

Steady-State Reduction Level of b_5. The b_5 reduction level was determined by differential spectroscopy at 28 °C. The assay mixture (1.2 mL, 120 pmol of 3A4) containing microsomes and substrate was divided equally between the two cuvettes. Oxidized b_5 was added in the sample cuvette at a b_5:3A4 molar ratio of 2:1. The b_5 differential spectrum was recorded 1 min after addition of NADPH (100 μM) to each cuvette, and the b_5 reduction level was deduced.

Reduction Kinetics. Reduction of ferric 3A4 to the ferrous−carbon monoxide form was measured at 28 °C under an anaerobic CO environment. Reduction of b_5 was measured aerobically and anaerobically. All studies were done on microsomal membranes using an Applied Photophysics SX-18MV instrument (Applied Photophysics, Leatherhead, U.K.). Kinetics were recorded using a photodiode array system. Five to fifteen individual spectrakinetics were averaged in each condition. Averaged data with and without NADPH were subtracted to eliminate most of the artifacts resulting from diffusion changes or mixing effects. Data were processed by spectral deconvolution using authentic ferrous−CO 3A4 and b_5 spectra as references. Experiments were carried out at 28 °C with a b_5:3A4 molar ratio of 2:1.

Numerical Simulation. The kinetic model for 3A4 uncoupling control by b_5 presented in Figure 5 was converted into the set of differential equations listed in Table 1. This set included, in addition to the reactions presented in Figure 5, five b_5 autoxidation steps by oxygen leading to pseudo-first-order conversion (rate constant = k_{17}) of all species including free or bound reduced b_5 into corresponding species including oxidized b_5. A step of pseudo-first-order reduction (rate constant = k_{18}) of free oxidized b_5 by various microso-

Table 1: Differential Equations and Rate Constants for Numerical Simulation of the Model

Differential equations :

d [P]/dt =-(k14*([Box] +[Brd]) +k1)*[P] +k15*([PBox] +[PBrd]) +k4*[POH] +k5*[PO] +k6*[PO2]
d [PO2]/dt =-k14*([Box] +Brd])*[PO2] +k15*([PO2Box]+[PO2Brd]) +k1*[P] -(k2 +k6)*[PO2]
d [PO]/dt =-k14*([Box] +[Brd])*[PO] +k15*([POBox]+[POBrd]) +k2*[PO2] -(k3 +k5)*[PO]
d [POH]/dt =-k14*([Box] +[Brd])*[POH]+k3*[PO]+k15*([POHBox]+[POHBrd]) -k4*[POH]
d [PBox]/dt =k14*[Box]*[P] +k5*[POBox] +k6*[PO2Box] +k10*[POHBrd] - (k11 +k15)*[PBox]
+k16*[POHBox]+k17*[PBrd]
d [PO2Box]/dt =k14*[Box]*[PO2] -(k6 +k7 +k15+k12)*[PO2Box] +k11*[PBox] +k17*[PO2Brd]
d[POBox]/dt =k14*[Box]*[PO]+k8*[PO2Brd] -(k5 +k15+k13)*[POBox]+k12*[PO2Box]+k17*[POBrd]
d [POHBox]/dt =k14*[Box]*[POH]+k9*[POBrd] -k15*[POHBox]+k13*[POBox]-k16*[POHBox]
+k17*[POHBrd]
d [PBrd]/dt =k14*[Brd]*[P]*+k7*[PO2Box]+k6*[PO2Brd] +k5*[POBrd] -(k15 +k11)*[PBrd]+k16*[POHBrd]
-k17*[PBrd]
d [PO2Brd]/dt =k14*[Brd]*[PO2]-(k6 +k8 +k15 +k12+k17)*[PO2Brd] +k11*[PBrd
d [POBrd]/dt =k14*[Brd]*[PO]-(k5 +k9 +k15+k13+k17)*[POBrd] +k12*[PO2Brd]
d [POHBrd]/dt =k14*[Brd]*[POH]-(k10 +k15+k17+k16)*[POHBrd] +k13*[POBrd]
d [Box]/dt =k15*([PBox]+[PO2Box]+[POBox]+[POHBox])-[Box]*k14*([P]+[PO2]+[PO]+[POH])+k17*[Brd]
-k18*[Box]
d [Brd]/dt =k15*([PBrd]+[PO2Brd] +[POBrd] +[POHBrd])-[Brd]*k14*([P]*+[PO2]+[PO]+[POH])-k17*[Brd]
+k18*[Box]
d [NADPH]/dt =(k1*[P]+k2*[PO2]+k3*[PO]+k4*[POH]+k11*([PBox]+[PBrd])+k12*([PO2Brd] +[PO2Box])
+k13*([POBox]+[POBrd])+k16*([POHBox]+[POHBrd]))/2
d[H_2O]/dt =k2*[PO2]+k4*[POH] +k10*[POHBrd] +k8*[PO2Brd] +k16*([POHBrd] +[POHBox])
+k12*([PO2Box]+[PO2Brd])
d [H_2O_2]/dt =k6*([PO2]+[PO2Box]+[PO2Brd])/2
d [SOH]/dt =k5*([PO]+[POBox]+[POBrd])

Rate constants (s^{-1}) :

Conditions	k1	k2	k3	k4	k5	k6	k7	k8	k9	k10	k11	k12	k13	k14[1]	k15	k16	k17	k18
Hb_5+S model 1	1.6	1.3	20	30	1	2.9	12	5	25	20	3.5	0.02	0.02	250	8	0.2	0.2	0.044
Hb_5-S model 1	0.4	-	-	-	0	-	-	-	-	-	0.6	-	-	-	-	-	-	-
Apo-b_5+S model 1	1.6	-	-	-	-	-	0	0	0	0	3.5	-	-	-	-	0	0	0
Apo-b_5+ S model 2	-	-	-	-	-	-	0	0	0	0	-	1.3	-	-	-	0	0	0

Substrate used was androstenedione 200 μM. (-) indicated identical values to ones in the line Hb_5+S. Rate constants are given in s^{-1}. [1]pseudo first order rate constant for b_5 binding to 3A4 at b_5 concentration of 0.15 μM. +S, substrate present ;-S, substrate absent ; Hb_5, holo-b_5 present ; Zn-b_5, zinc b_5 present ; model 1 : simulation in the membrane bound state ; model 2 ; simulation in reconstituted system.

mal redox enzymes was also introduced to account for the background of b_5 reduction in the absence of 3A4. An interactive simulation program described previously (*56*) was used to solve the pre-steady-state and steady-state behaviors of the model using rate constants listed in Table 1. The b_5 concentration used for simulation was 0.3 μM for 2:1 b_5 to P450 molar ratio conditions. The iterative resolution method with automated step control used for solving differential equations guarantees a relative error of less than 10^{-3} on any calculation.

RESULTS

Analysis of the P450 3A4 Catalytic Cycle Based on Electronic, Oxygen, and Substrate Balances. Determination in natural membranes of substrate, oxygen, and electronic balances associated with P450 3A4 functions requires that nonspecific NADPH oxidation and hydrogen peroxide formations (due to endogenous yeast proteins) be limited compared to the P450 related contributions. Membranes containing a high 3A4 content (close to 1 nmol/mg of membrane protein) and adapted human CPR:P450:b_5 molar ratios (1:10:20) were thus prepared using a high-efficiency yeast expression system. With this system simulating the liver situation, data could be easily corrected for P450-independent backgrounds and for self-decomposition of accumulated hydrogen peroxide in each experimental condition used (see Experimental Procedures).

P450 uncoupling depends on both the nature of the substrate and the presence of b_5 (*15, 57*). Electronic balance for microsome-bound 3A4 was analyzed with six different substrate conditions, with and without human b_5 (Table 2). Control experiments using a yeast strain deleted for the endogenous microsomal b_5 gene indicated that yeast b_5 did not interact in a detectable way with 3A4 nor modify the effect of human b_5 (data not shown). A significant rate of 3A4-dependent NADPH oxidation [close to 20 nmol (nmol of P450)$^{-1}$ min^{-1}] was observed in the absence of substrate. Cyclosporin reduced the rate of NADPH oxidation to the limit of quantification (4 min^{-1}), while steroids increased it up to 60 min^{-1}. Nifedipine and quinidine have intermediate behaviors. However, we found no relationship between these rates and the extent of 3A4 spin-shift induced by substrate binding (data not shown). These data contrasted with previous reports on $P450_{cam}$ showing that reduction of ferric P450 was triggered by substrate-induced spin changes (*43, 58*).

Table 2: P450 3A4 Substrate, Oxygen, and Electronic Balances[f]

substrate	without cytochrome b_5				with cytochrome b_5[a]			
	NADPH[b] (min^{-1})	H_2O_2[c] (min^{-1})	water[d] (min^{-1})	product(s)[e] (min^{-1})	NADPH[b] (min^{-1})	H_2O_2[c] (min^{-1})	water[d] (min^{-1})	product(s)[e] (min^{-1})
none	20 ± 1.2	4 ± 0.5	16 ± 2	0	18 ± 0.5	6 ± 1	12 ± 2	0
cyclosporin	4.2 ± 1.4	1 ± 1	3 ± 2	0.16 ± 0.05	5.6 ± 1	1 ± 1	4.6 ± 2	0.25 ± 0.05
nifedipine	20 ± 3	6.5 ± 1.5	13.5 ± 5	1.6 ± 0.1	24 ± 2	5.1 ± 0.4	19 ± 2.5	3.1 ± 0.2
testosterone	51 ± 1	12 ± 1	39 ± 2	1.7 ± 0.2	51 ± 2	6.7 ± 0.4	44 ± 3	7.9 ± 0.3
androstenedione	64 ± 3	22 ± 2	42 ± 5	1.0 ± 0.1	67 ± 2	14 ± 2	53 ± 4	7.4 ± 0.3
quinidine	22 ± 1	6.4 ± 0.8	15.6 ± 2	0.24 ± 0.05	16 ± 2	3.8 ± 0.6	12 ± 3	0.58 ± 0.06

[a] b_5 is added at a 2:1 molar ratio compared to P450. [b] For NADPH oxidation, data were corrected to subtract background not related to P450-dependent activity as described in Experimental Procedures. [c] No background of hydrogen peroxide formation exceeding the limit of detection (equivalent to about 1 min^{-1} in the table) was detected with P450 free microsomes. [d] Water formation was deduced from the electronic balance assuming that one atom of dioxygen was incorporated into the substrate (monooxygenase reaction). [e] pmol of product(s) formed (sum of substrate metabolites) (pmol of P450)$^{-1}$ and min^{-1}. [f] Microsomal fractions corresponding to 50 pmol of P450 3A4 were incubated at 28 °C in standard buffer for 15 min. Incubations were performed using 100 μM NADPH and 200 μM substrate (testosterone, androstenedione, quinidine, and nifedipine) or 70 μM cyclosporin A.

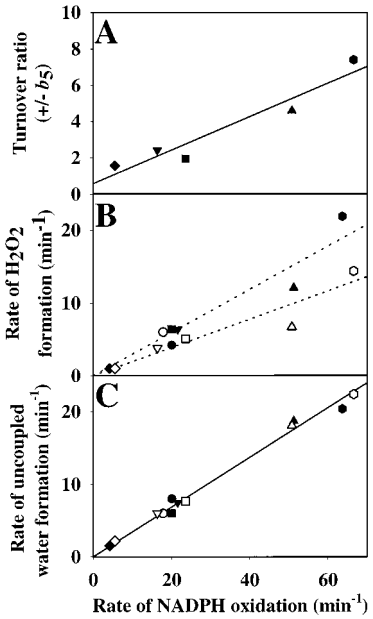

FIGURE 1: Relationship between NADPH oxidation, uncoupled water, and hydrogen peroxide formations and effect of b_5 on substrate oxidation. Microsomal fractions (50 μg of protein) containing 50 pmol of P450 3A4 were incubated at 28 °C (●) without substrate and with (◆) cyclosporin, (■) nifedipine, (▲) testosterone, (⬢) androstenedione, and (▼), quinidine in standard buffer containing 100 μM NADPH. Substrate concentration was 200 μM, except for cyclosporin (70 μM). (A) The effect of b_5 on substrate oxidation was calculated on the basis of a 15 min incubation (linearity was checked). (B) Hydrogen peroxide formation was monitored, and the initial rate of formation was calculated as described in Experimental Procedures on the basis of data obtained after 0, 1, 2, 3, and 4 min of incubation. This calculation allowed to correct for self-catalyzed or catalyzed decomposition of accumulated hydrogen peroxide. Reported values represent only the P450 3A4 dependent contributions. (C) The rate of uncoupled water formation (bielectronic reduction of the ferryl−oxo complex to water) was calculated using the electronic balance of the overall reaction as follows: rate of formation of uncoupled water = $(V_{NADPH} - V_{H_2O_2} - V_{product})/2$ (see text), where V_{NADPH}, $V_{H_2O_2}$, and $V_{product}$ were the rates of NADPH oxidation, hydrogen peroxide formation, and total metabolite formation, respectively. In all panels open and closed symbols represent experiments in the presence and in the absence of b_5, respectively.

Table 2 indicates that membrane-bound 3A4 is a widely uncoupled enzyme. In the absence of b_5, the fraction of productive catalytic cycles (ratio between rates of product formation and NADPH oxidation) ranged from 1% to 8%, depending on the substrate tested, and uncoupling occurred in similar amounts by production of hydrogen peroxide and water (Figure 1B,C). The rate of product formation was enhanced by b_5 for all substrates tested, and the extend of the effect correlated with the ability of a given substrate to enhance the rate of NADPH oxidation (Figure 1A). In the same substrate conditions, the rate of hydrogen peroxide formation was generally reduced in the presence of b_5 while the rate of NADPH oxidation remained unchanged (Figure 1B).

Scheme 1: Simplified Catalytic Cycle for P450 3A4[a]

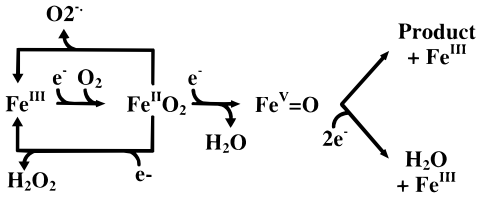

[a] Fe^{III}, $Fe^{II}O_2$, and Fe^{V}=O represent the P450 in the oxidized state, the ferrous−dioxygen complex, and the reactive high-valent complex, respectively.

P450-dependent water formation occurs at two levels in the P450 catalytic cycle (Scheme 1): the heterolytic cleavage of the O−O bond within the peroxy compound (*43*) and the reduction of the ferryl−oxo species (*45*, *46*). Experimentally, the rate of water formation cannot be determined directly but was calculated from the oxygen and electronic balances assuming that only one atom of dioxygen was incorporated into the substrate (see Figure 1 legend). The rate of formation of uncoupled water resulting from ferryl−oxo P450 reduction thus calculated (Figure 1C) was proportional to the rate of NADPH oxidation but independent of the presence of b_5.

Following P450 catalytic cycle initiation by electron transfer from CPR to ferric 3A4, two-electron requiring cycles (product or hydrogen peroxide forming) or four-electron requiring cycles (uncoupled water forming) are possible. The average number of electrons required to complete one initiated P450 cycle was calculated as $n_{NADPH} = 2V_{NADPH}/(V_{NADPH} + V_{H_2O_2} + V_{product})$ from the steady-state data (V_{NADPH} and $V_{product}$ were rates of NADPH oxidation and total metabolite formation, respectively). With and without b_5, rather similar values (3.0 ± 0.5) were obtained for all substrates considered. This suggested that relative proportions of two- and four-electron cycles were similar

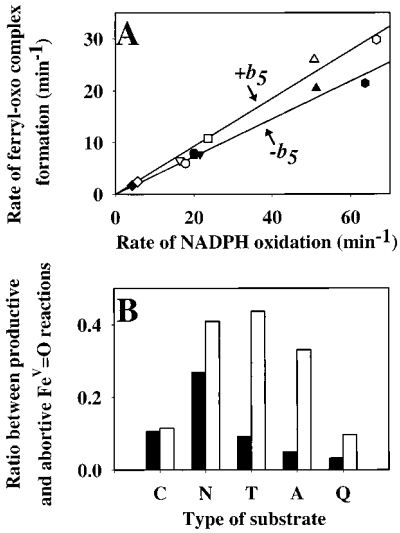

FIGURE 2: Effects of b_5 on the formation of the P450 3A4 ferryl−oxo complex and on its partition between productive and abortive decomposition. (A) Rates of ferryl−oxo complex formation were calculated as the sum of the rates of product and uncoupled water formations (●) without substrate and with (◆) cyclosporin, (■) nifedipine, (▲) testosterone, (⬢) androstenedione, and (▼) quinidine. (B) Partition ratios between productive and abortive reactions at the level of the ferryl−oxo complex were calculated from Table 2 (rate of product formation) and Figure 1 (uncoupled water formation) data. Open and closed boxes and symbols represent experiments in the presence and in the absence of b_5, respectively. Substrates: C, cyclosporin; N, nifedipine; T, testosterone; A, androstenedione; Q, quinidine.

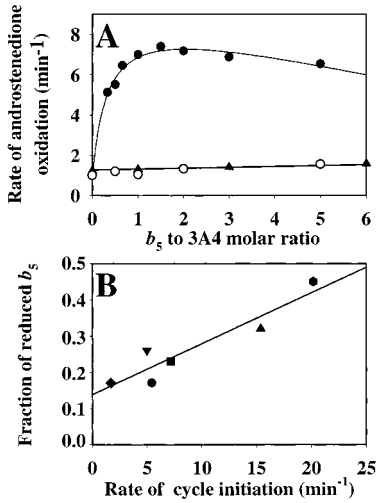

FIGURE 3: Relationship between b_5 redox properties and substrate oxidation. (A) P450 3A4 containing microsomes were incubated at 28 °C as described in Table 2 in the presence of increasing concentrations of Fe-b_5 (●), Zn-b_5 (▲), or apo-b_5 (○). Rates were calculated on the basis of the sum of all androstenedione metabolites. (B) The rate of cycle initiation was calculated as the ratio between the rate of NADPH oxidation and the average number of electrons used per initiated cycle. The fraction of reduced b_5 was determined by differential spectrophotometry 1 min after NADPH addition. This value was stable for 15 min. Conditions: (●) without substrate and with (◆) cyclosporin, (■) nifedipine, (▲) testosterone, (⬢) androstenedione, and (▼) quinidine.

for all substrates and did not depend on b_5. Therefore, changes in the rate of NADPH oxidation reflected changes in the rate of cycle initiation by ferric 3A4 reduction to the ferrous−dioxygen complex. In contrast to substrates, b_5 did not change the rate of NADPH oxidation, suggesting that it did not affect the rate of electron transfer from CPR to ferric 3A4. We then questioned whether the b_5 enhancing effect could result from a role on later steps in the catalytic cycle.

Modulation by b_5 of Ferryl−Oxo Complex Partition between Productive and Abortive Reactions Could Appear Incompatible with a Pure Redox-Based Mechanism. Formation rates and partition of the ferryl−oxo complex between productive and abortive reactions were calculated on the basis of the mechanism shown in Scheme 1 and electronic and matter balances. The rate of the ferryl−oxo complex formation can be simply deduced from the sum of rates of product(s) and uncoupled water ((Δ[NADPH] − Δ[H_2O_2] − Δ[products])/2) formations. The b_5-dependent increase (about 30%) of the rate of ferryl−oxo complex formation (Figure 2A) resulted from a corresponding decrease in the rate of hydrogen peroxide formation as the rate of ferrous−dioxygen complex formation did not depend on b_5 (Figure 1). Nevertheless, this limited enhancement cannot account for the large b_5 effect (up to 7-fold) observed on the rates of steroid oxidation. Consequently, influence of b_5 on the partition between productive and abortive decomposition of the ferryl−oxo complex was considered. This ratio can be simply evaluated as PR = 2Δ[product]/(Δ[NADPH] − Δ-[H2O2] − Δ[product]). Figure 2B illustrated that this ratio highly depended on the nature of the substrate as expected from a differential reactivity of the different substrates with the activated oxygen species. In the presence of b_5, this ratio was increased from 1.1- to 6.6-fold (lower and upper limits: cyclosporin and androstenedione, respectively). Therefore, most of the enhancing effect of b_5 appeared to be related to a change in the partition of ferryl−oxo 3A4 between productive (oxidation of substrate) and abortive (reduction to water) reactions.

This result was surprising considering the postulated role of b_5 as an alternate electron donor to P450. Particularly, reduced b_5 was expected to favor reduction of the ferryl−oxo complex to water (*59*) while not affecting the rate of the active oxygen reaction with substrate. Experimental data contrasted with this prediction and supported an alternate scheme involving a 3A4 conformational change induced by b_5 binding and affecting reactivity of the 3A4 ferryl−oxo complex with substrate. We attempted to reproduce in natural membrane-bound conditions the 3A4 activation by apo-b_5 previously reported in reconstituted systems involving purified enzymes and phosphatidylcholine micelle based structures (*31*).

Redox-Active b_5 Was Required for 3A4 Activation in Membrane-Bound Conditions, and the Redox State of b_5 Was Modulated by the P450 Catalytic Cycle. Experiments (Figure 3A) were carried out with natural or with redox inactive b_5 (heme free, zinc containing, or cobalt containing). The enhancing effect of b_5 (close to 8-fold on androstenedione oxidation) was saturable for a b_5:P450 molar ratio in the order of 1:1. A large excess of Fe-b_5 led to a slight decrease in the activation. Surprisingly, similar experiments with apo, zinc, or cobalt reconstituted b_5 evidenced only a very limited, if significant effect in membrane-bound conditions. Such an observation appeared inconsistent with a redox-independent mechanism for the b_5-dependent modulation of ferryl−oxo complex partition (Figure 2B). Binding of testosterone or androstenedione to 3A4 was monitored by analysis of P450 spectral perturbation in the absence and

the presence of Fe- or Zn-b_5. Data indicated the absence of any detectable 3A4 spin equilibrium perturbation or substrate affinity change upon b_5 binding, thus the absence of any detectable conformational effect. These results on the membrane-bound system contrasted with a previous report based on experiments with purified enzymes and micelle reconstituted systems (*23*, *25*, *30*).

To evaluate the extent of redox exchanges between 3A4 and b_5 during the P450 catalytic cycle, the redox state of b_5 was analyzed in the presence and in the absence of membrane-bound 3A4. We previously evidenced that the presence of P450 substrates modified electron flow from CPR to 3A4 (Figures 1 and 2). Consequently, modulation of the b_5 redox state by the presence of 3A4 substrates was expected if b_5 rapidly exchanges electrons with 3A4. The limited reduction level of b_5 (close to 15%) was observed in aerobic steady-state conditions in the presence of coexpressed human CPR and NADPH. This level was found roughly equal in membrane containing or deprived of 3A4 when no substrate was present. Surprisingly, the presence of the 3A4 substrate was required for the P450-dependent increase in the b_5 reduction level, with a maximal reduction level reaching 45% in the presence of a saturating concentration of androstenedione (Figure 3B). This phenomenon was dependent on the substrate nature and concentration. A correlation appeared between the extend of b_5 reduction and the rate of P450 cycle initiation (Figure 3B) as evaluated by the ratio between the NADPH oxidation rate and the average number of electrons used per initiated cycle (Table 2). Controls performed with microsomes differing only by the absence of 3A4 coexpression did not show any substrate dependence of the b_5 reduction state. Furthermore, the enhancing effect of b_5 on substrate oxidation rates was found linearly related with the steady-state level of reduced b_5 (data not shown). Together, these results strongly suggested that electron exchanges between b_5 and 3A4 as well as b_5 redox states were tightly linked with activities enhancing properties of b_5 in the membrane-bound state.

Rapid Kinetic Analysis Confirmed That Fast Electron Exchanges Occurred between 3A4 and b_5 within a Single Turnover Duration. To further confirm that the observed dependence of the b_5 redox state on the 3A4 catalytic cycle was related to electron exchange occurring within the time range of a catalytic cycle, the course of the b_5 redox state was analyzed by rapid kinetic techniques. Experiments in the membrane-bound system was rendered difficult by the strong light scattering properties of natural constituents. These problems were solved as described in Experimental Procedures. In a first experiment, the time course of b_5 reduction following NADPH addition to membranes containing the human CPR, 3A4, and human b_5 (0.1:1:2 molar ratios) was analyzed in air and substrate (androstenedione) saturated conditions. We observed a rapid biphasic (rate constants: 3.0 and 0.33 s^{-1}) but partial reduction (about 50%) of b_5 before a stable stationary phase was reached (Figure 4A, trace a). When 3A4 was omitted (no coexpression), a signal was still present (Figure 4A, trace b) but with a much lower amplitude (2.5−3-fold less). This residual signal was clearly related to 3A4-independent b_5 reduction as no signal was observed in a second control omitting b_5 (Figure 4A, trace c). Interestingly, when the 3A4 substrate (androstenedione) was omitted, dependence of the amplitude of the b_5 reduction trace on the 3A4 presence was lost. This indicated that although a part of the b_5 reduction in membrane resulted from 3A4-independent phenomena, the major part of the reduction signal in the presence of androstenedione required the presence of 3A4. The amplitudes of b_5 reduction measured in rapid kinetic studies were found identical within experimental error to values measured in steady-state experiments by differential spectroscopy and exhibited the same dependence on substrate nature as previously described in Figure 3B. We concluded that a 3A4 and substrate-dependent reduction of b_5 occurred within the first 2 s following NADPH addition. This rate is much faster than the 3A4-independent b_5 autoxidation (0.08−0.2 s^{-1}). Consequently, the limited and substrate-dependent b_5 reduction (15−45%) at the kinetic plateau requires compensatory electron transfers involving 3A4 as both electron donor and acceptor for b_5. In such conditions, the 3A4 substrate dependence of the b_5 redox state resulted from a substrate-dependent modulation of the balance between the electron source and sink by 3A4.

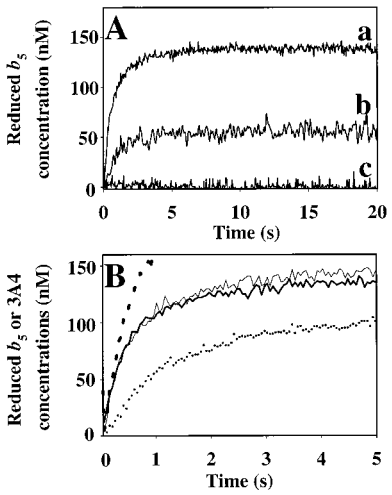

FIGURE 4: Kinetics of reduction of b_5 and ferric 3A4 in microsomal membranes. All data were processed as described in Experimental Procedures. (A) Kinetics of reduction of b_5 (300 nM) in 3A4 (150 nM) containing membranes and air-saturated buffer in the presence of 200 μM androstenedione (trace a). Same experiment in 3A4-free membranes (trace b) and in 3A4 and b_5-free membranes (trace c). Reduced b_5 concentrations were calculated by spectral deconvolution. (B) Kinetics of reduction of 3A4 (150 nM) and b_5 (300 nM) by NADPH in anaerobic, carbon monoxide saturated buffer. Dotted and thin solid lines represent respectively the formation of reduced carbon monoxide 3A4 and of reduced b_5 in the same experiment. Reduced enzyme concentrations were calculated by deconvolution of spectrakinetic data. The dashed line represents the sum of the two previous kinetic experiments (3A4 and b_5 reductions). The bold solid line represents the formation of reduced carbon monoxide 3A4 in a control experiment when b_5 was absent from membranes.

To further confirm that the 3A4-dependent b_5 reduction involved a direct electron transfer between 3A4 and b_5 and not a facilitated interaction between b_5 and the reductase, the experiment was repeated in anaerobiosis and the presence of carbon monoxide to trap reduced 3A4 into easily observable species. Deconvolution of spectrakinetic traces was used to fully separate b_5, P450, and background contributions (control experiments not shown). In the absence of b_5, full reduction by NADPH of 3A4 into its Fe^{II}−CO complex occurred with rate constants of 2.6 and 0.36 s^{-1} (Figure 4B). When the experiment was repeated in the presence of b_5,

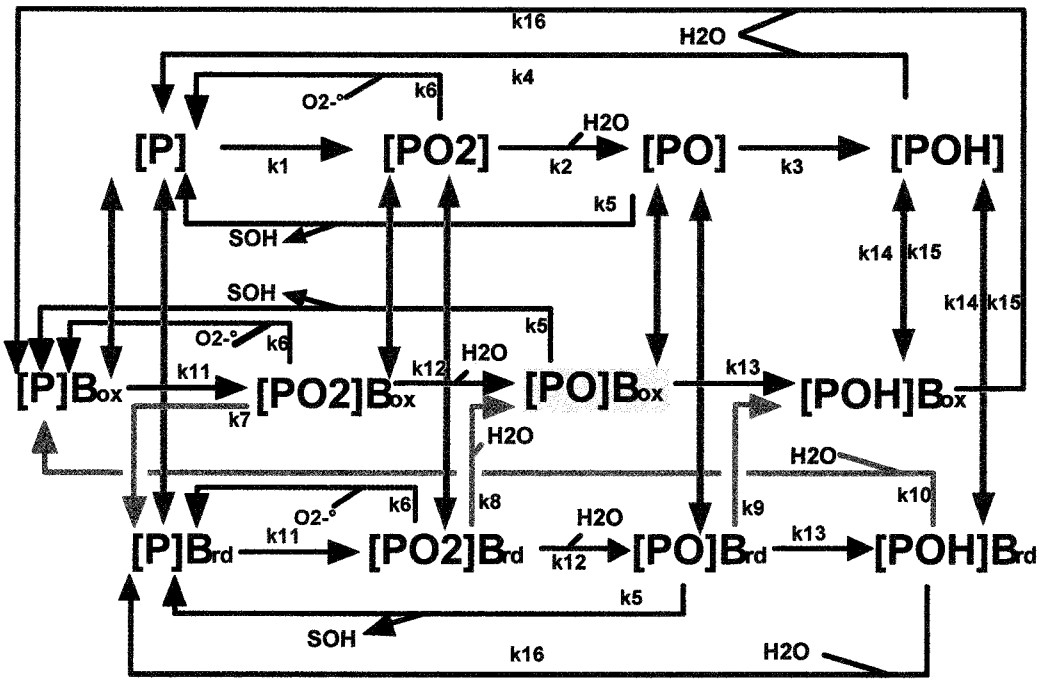

FIGURE 5: 3A4 kinetic model for b_5 effects. [P], [PO2], [PO], and [POH] represent P450 3A4 Fe^{III}, $Fe^{II}O_2$, Fe^{V}=O, and Fe^{IV}−OH complexes, respectively. B_{ox} and B_{rd} represent oxidized and reduced b_5, respectively. Complexes between 3A4 and b_5 in their different redox states are indicated by $[P]B_{ox}$, $[PO2]B_{ox}$, $[PO]B_{ox}$, $[POH]B_{ox}$, $[P]B_{rd}$, $[PO2]B_{rd}$, $[PO]B_{rd}$, and $[POH]B_{rd}$. Black and green arrows indicate kinetic steps involving electron transfer between CPR and 3A4 and between 3A4 and b_5, respectively. SOH represents product formation. Blue arrows indicate kinetic steps not involving electron transfer, and red arrows indicate binding or dissociation steps between 3A4 and b_5. Substrate and reductase binding steps are not explicitly shown and are embedded into the apparent first-order rate constants.

the initial rate of 3A4 reduction was found strongly reduced. Interestingly, b_5 was reduced at a rate rather similar to the value observed for 3A4 in the absence of b_5 (with rate constants of 2.5 and 0.33 s^{-1}). The sum of reduced b_5 and reduced 3A4 concentrations was calculated and the resulting trace (Figure 4B) compared to the trace in the absence of b_5. The two traces exhibited the same initial velocity within experimental errors, consistently with a redistribution of the electron flow between 3A4 and b_5 in the 3A4−b_5 complex. In addition, the shapes of the traces were consistent with a mechanism involving electron transfer from 3A4 to b_5 with a first-order rate constant fast enough compared to the rate constant of 3A4 reduction by CPR, thus slowing down Fe^{II}−CO complex formation due to electron redistribution. The rates of reduction of both 3A4 and b_5 were enhanced by the presence of androstenedione (3A4, 300 and 89 nM s^{-1} with and without substrate, respectively; b_5, 320 and 147 nM s^{-1} with and without substrate, respectively). The correlated increase in the b_5 and 3A4 reduction rates by substrate was not expected for a mechanism in which b_5 binding to 3A4 would favor direct b_5 reduction by CPR. In such a case, increased electron flow to 3A4 would be expected to decrease the b_5 reduction rate due to competition for CPR. This suggested that electron flow was going first from CPR to 3A4 (rate increased by substrate) and then from 3A4 to b_5. In addition, stopped-flow experiments indicated that b_5 did not enhance the rate of reduction of membrane-bound ferric 3A4 in contrast with a previous report using a reconstituted system (*31*).

Together, these experiments supported the occurrence of extensive electron exchange between 3A4 and P450 within a time range shorter than the one for a single turnover. These data raised the possibility of a redox-based mechanism explaining all b_5 features, including the effect on the partition ratio of ferryl−oxo between productive and abortive mechanisms. We then decided to search for a single kinetic model accounting for all of these apparently contradictory data.

Design of a 3A4 Kinetic Model for b_5 Effects. Tested models were based on a simplified kinetic scheme for P450 involving the resting Fe^{III} state, the ferrous−dioxygen complex, and the iron−oxo species. The Fe^{II} intermediate was not considered as its conversion into the ferrous−dioxygen complex was not kinetically limiting in air-saturated conditions. The Fe^{III}−peroxy complex was also masked, as this species did not belong to a critical kinetic branch point in the oxygen-dependent mechanism. Finally, the simplest model allowing simulation of experimental data was presented in Figure 5. This model was constituted by three copies (b_5 free, reduced b_5 bound, oxidized b_5 bound) of the minimal kinetic scheme interlinked by binding and electron-transfer steps involving b_5. The half-reduced ferryl−oxo complex explicitly appeared on the scheme because it belonged to cross-points in the mechanism. CPR binding steps are not explicitly represented as the experiments involved similar CPR to P450 ratios and thus similar saturation. Reductase saturation status and rates of electron transfer to 3A4 were therefore embedded into apparent kinetic constants (this reduced the number of species from 24 to 12). An additional simplification was formation of hydrogen peroxide only from dismutation of superoxide released from the ferrous−dioxygen complex. Direct release from the masked peroxy−ferric intermediate was not explicit but again can be embedded in the model by use of a suitable coefficient (between 1 and 2) for hydrogen peroxide formation by uncoupling. Controls indicated that the exact value of this coefficient was without consequence on the model prediction provided some minor readjustment of rate constants.

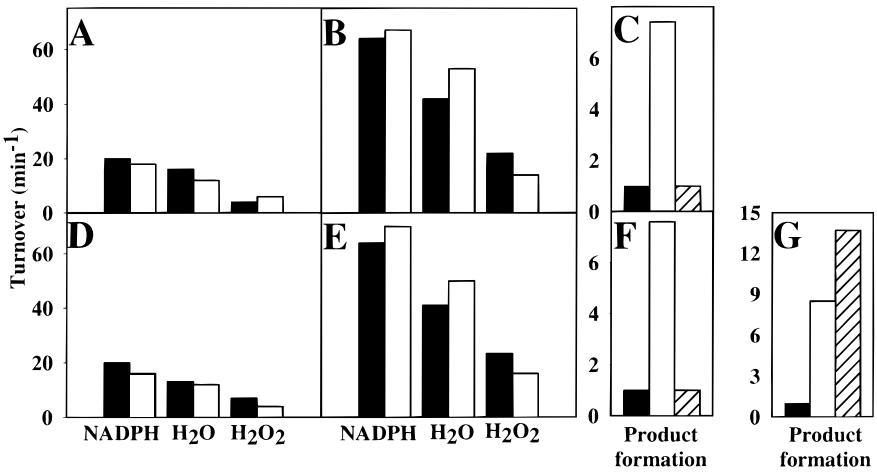

FIGURE 6: Comparison between experimental and simulated data for product, hydrogen peroxide, and total water formation. (A) Experimental data obtained without substrate. (B, C) Experimental data obtained in the presence of 200 μM androstenedione. (D−F) Simulated data for the same conditions as in (A−C), respectively, using kinetic parameters from Table 1, model 1 (simulation of our experimental conditions). (G) Simulated data obtained according to Table 1, model 2. Equivalent data of (D) and (E) were not shown for these conditions. Closed boxes represent experiments without b_5. Open boxes represent experiments done with iron-b_5. Hatched boxes represent experiments with redox-inactive b_5 (zinc- or apo-b_5).

Model Adjustment to Rapid Kinetics and Simulation of Steady-State Experimental Data. Global adjustment of the model was performed in order to reach a minimum set of rate constants reasonably fitting all experimental data. To limit the number of independent constants, the following simple rules were applied: (i) for reactions not involving electron transfer, like ferrous−dioxygen self-decomposition or substrate hydroxylation by the ferryl−oxo complex, identical rate constants were taken whatever the b_5 complexation status; (ii) similarly, k_{on} and k_{off} for b_5 binding and dissociation were taken independent of 3A4 and b_5 redox states; (iii) for electron-transfer reactions involving the CPR, identical rate constants were taken for similar steps in b_5 complexes irrespective of the b_5 redox states while different rates were allowed for b_5-free and bound complexes to account for possible steric interactions between the b_5 and reductase binding sites. Constant optimization (Table 1) was performed to simulate experiments involving or not androstenedione as substrate: the absolute order of magnitude for k_1 (reduction of ferric 3A4 by CPR) and k_7 (reduction of b_5 by ferrous−dioxygen 3A4) was evaluated on the basis of Figure 4 rapid kinetic data; the k_6/k_2 ratio (controlling H_2O_2 formation) and k_5/k_3 ratio (controlling product formation) were adjusted to fit Table 1 data; the k_{14}/k_{15} ratio (controlling b_5 affinity) was optimized for Figure 3A fitting; the k_7/k_8 ratio was adjusted for fitting b_5 reduction levels; k_{12}, k_{13}, and k_{15} were adjusted to simulate holo- and apo-b_5 effects consistent with experimental data; k_{16} was arbitrary chosen equal to k_{13}; the k_{11}/k_1 ratio was adjusted to fit variations of NADPH oxidation rates with and without b_5. Finally, all constants were tuned by a trial and error method for global simulation of all experimental data. To account for 3A4-independent b_5 redox reactions, an additional autoxidation step (k_{17}) was introduced in the model (not shown on Figure 5 but included in the Table 1 equations) and adjusted from experimental data in the absence of 3A4. Similarly, to simulate the 3A4-independent b_5 reduction (Figure 4A), a P450-independent b_5 reduction step (k_{18}) was added and adjusted for optimal fit of the b_5 reduction level in the absence of 3A4. However, exact values or even omission ($k_{17} = k_{18} = 0$) of these two constants were found to have only marginal consequences on predicted b_5 effects.

Except for k_1 and k_{11} (reduction of ferric 3A4 by CPR) that were chosen to depend on substrate presence and saturation, the same set of rate constants was used to simulate all conditions (plus or minus substrate and various b_5 saturation). As illustrated in Figure 6, this model (Table 1, model 1) tightly predicted experimental NADPH, H_2O_2, H_2O, and product formations in the four limit conditions (with and without substrate and b_5). Interestingly, the absence of effect of redox-inactive b_5 (apo- or zinc-b_5) can be simulated simply by zeroing k_7, k_8, k_9, and k_{10} (b_5-dependent electron-transfer reactions). When b_5 concentration was varied in the model, saturable activation was predicted (Figure 7A) and compared fairly well with experimental data (Figure 3A). Moreover, the model well predicted the 3A4 and substrate dependence of the b_5 reduction level (data not shown). Therefore, predictions were consistent with all the experimental data within the limits of experimental errors and the rather approximate adjustment of the model rate constants.

Analysis of Molecular Mechanisms Controlling 3A4 Activation by Apo- and Holo-b_5. On the basis of the fairly good fitting of experimental data by the model, we questioned the molecular phenomena controlling b_5 effects and particularly the observation of the b_5-induced change in the partition ratio at the ferryl−oxo complex level. The b_5-induced changes in the rate of ferryl−oxo complex formation and in the partition ratio of the ferryl−oxo complex between productive and abortive reactions were calculated for the model (Figure 7B,C) in the same way as for experimental data (Figure 2A,B). While experimental and predicted b_5 effects on the rate of product formation were large (up to 8-fold for androstenedione), experimental b_5-dependent modulation of the rate of ferryl−oxo species formation was limited (about 30%; Figure 2A). This phenomenon was nicely reproduced by the simulation (Figure 7B). Similarly, the increase in the partition ratio of ferryl−oxo reduction to product compared to water was experimentally observed (Figure 2B) and well simulated (Figure 7C). Moreover, this change occurred experimentally without an increase in the

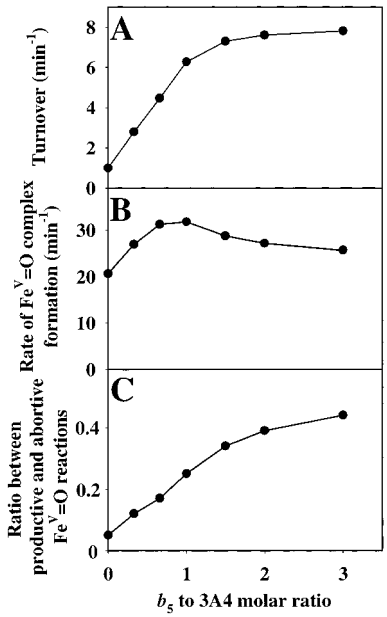

FIGURE 7: Simulated effects of b_5 on substrate oxidation (A) and on rate of formation (B) or partition (C) of the ferryl−oxo complex in the presence of androstenedione. Simulation was performed with the Table 1, model 1, rate constant set. Rules for calculation of ferryl−oxo complex formation and partition were the same as those for the experimental data in Figures 1−3.

absolute rate of water formation (Figure 1C), and this feature was also simulated (Figure 6D,E). This illustrated that the shift of ferryl−oxo partition to product oxidation can be fully simulated by a model based on the b_5 redox properties (this effect was abolished in the simulation of the zinc-b_5 effect).

Therefore, it was of interest to analyze adjusted rate constants in model 1 to determine which kinetic steps controlled this unexpected effect. Three major features appeared during the trial and error adjustment process: (i) the b_5 enhancing effect was abolished when k_{13} (reductase to b_5−ferryl−oxo electron transfer) was chosen to have a nonlimiting value compared to k_5 (substrate oxidation by the ferryl−oxo complex); (ii) when k_{13} was chosen limiting, not only holo-b_5 but apo- and zinc-b_5 were strong activators of 3A4 provided that k_{12} (electron transfer from reductase to the b_5−ferrous−dioxygen complex) was high enough compared to k_8; (iii) the ratio k_{15}/k_5 (k_{15}: dissociation rate of b_5 in the 3A4−b_5 complex) controlled the extent of the b_5 effect (Figure 8). Interestingly, with the parameters of Table 1, model 1, the fraction of oxidized b_5 in the b_5−ferryl−oxo complexes was predicted to be much higher than the fraction of oxidized b_5 in the free state or bound to Fe^{III} or $Fe^{II}O_2$ 3A4. With androstenedione as substrate, the calculated reduction level of b_5 bound to the ferryl−oxo complex was 8% compared to 40% for free b_5. This phenomenon was not related to a different affinity of reduced and oxidized b_5 (these were taken identical in the model for all 3A4 species) but to a kinetic discrimination when k_{13} and k_{15} were limiting. This kinetic discrimination occurred because in such conditions oxidized b_5−ferryl−oxo complex mainly decomposed via substrate oxidation (low k_{13}/k_5 and k_{15}/k_5 ratios) whereas the reduced b_5−ferryl−oxo complex can hardly form (low k_{12}/k_8 ratio). This caused a selective accumulation of the oxidized b_5−ferryl−oxo complex and consequently a specific increase in product formation without increase in water formation. In such conditions, redox-inactive b_5 cannot be

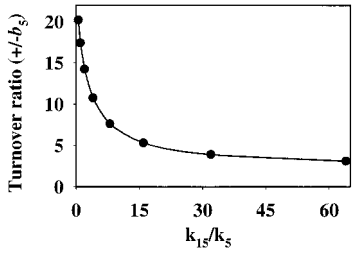

FIGURE 8: Relationship between the values of the rate constants for b_5 dissociation (k_{15}) and simulated iron-b_5 effect on androstenedione oxidation. Simulations were performed using rate constants from Table 1, model 1, except for constants of k_{14} and k_{15}. For all values of k_{15} tested, the corresponding values of k_{14} were chosen in order to maintain a constant k_{14}/k_{15} ratio (i.e., the same affinity between 3A4 and b_5). The *X*-axis was labeled as a k_{15}/k_5 ratio because this ratio and not the absolute value of k_{15} was found to be the determining parameter (practically, k_5 was kept constant for the simulation).

the activator because the b_5−ferryl−oxo complex cannot accumulate when k_{12} was low and $k_8 = 0$ (redox-inactive b_5). In contrast, assuming a situation where k_{12} was nonlimiting (Table 1, model 2), activation by zinc- or apo-b_5 could occur with an efficiency similar to that of holo-b_5 (Figure 6G) as reported by Yamazaki et al. in the reconstituted system (*31*).

At the molecular level, a null or low value for k_{12} and k_{13} implied that reductase cannot efficiently donate an electron to ferrous−dioxygen and ferryl−oxo complexes when b_5 was bound irrespective of its redox state. In contrast, reduction of the ferric 3A4 by the reductase (k_{11}) must remain efficient when 3A4 was bound to b_5. This was suggested experimentally by rapid kinetic experiments (Figure 4B), by the absence of a b_5 effect on NADPH oxidation rates (Figure 1), and theoretically by the observation that k_{11} must be at least as high as k_1 (reductase electron transfer to ferric 3A4) for acceptable simulation. Nevertheless, slight inhibition of activity by a large excess of b_5, as shown in Figure 3A, might indicate a partial interaction between CPR and b_5. Therefore, the model presented allowed fairly suitable simulation of all experimental data available and gave a molecular basis for analysis.

DISCUSSION

The present work reported a detailed analysis of the mechanism of b_5 effects on 3A4 activities based on electronic, substrate, and oxygen balances in membranes containing human P450 reductase, 3A4, and human b_5. Membrane-bound tunable CPR−3A4−b_5 systems were constituted using a recombinant yeast expression. In these conditions, 3A4-dependent substrate oxidation accounted for only 1−8% of total electron flow in the absence of b_5 and uncoupling occurred almost equally by P450-dependent water and hydrogen peroxide formations. The presence of a saturating amount of b_5 increased coupling up to 7-fold when androstenedione was the substrate. Results indicated that the nature of the substrate strongly modulated 3A4-dependent rates of NADPH oxidation. These changes resulted mainly from modulations of the flow of the first electron transfer between CPR and the ferric 3A4. The electron flow for this step was independent of the presence of b_5.

Conformational effects of b_5 were suggested on the basis of the observation that binding of b_5 induced a high-spin

shift of $P450_{LM2}$ facilitating substrate binding and electron transfers (*23*). Such finding was confirmed by the recent observation that heme-depleted b_5 can also strongly enhance CPR to 3A4 electron transfer in the reconstituted system (*9*, *31*). However, in the membrane-bound system, no detectable effect of b_5 on steroid affinity to membrane-bound ferric 3A4 and on P450 spin state equilibrium was evidenced. Furthermore, our experiments with apo-, Zn-, or Co-b_5 analogues did not show any significant enhancement of 3A4 activity in membrane-bound conditions. These contradictory results might relate to different P450 environments in compared experiments; i.e., reconstituted and membrane-bound systems but suitable molecular explanations were to date absent.

In our experimental conditions, b_5 effects resulted from a combination of an increase in the flow of ferryl−oxo complex formation and a modulation of ferryl−oxo complex partition. The first effect was a direct consequence of a decrease in the rate of hydrogen peroxide formation. Electron transfer from reduced b_5 to the ferrous−dioxygen complex favored a productive reduction of this complex competitive with its decomposition by superoxide release and dismutation into hydrogen peroxide. However, the observed b_5-dependent increase in the rate of ferryl−oxo complex formation was rather limited (30%) and cannot account for the large effect (up to 700%) observed in the rates of steroid oxidation. In contrast, a strong increase in the partition of the ferryl−oxo complex toward substrate oxidation was evidenced without a significant change in the rate of water formation. Two opposite schemes can be considered for the molecular mechanism of partition changes: conformational or redox-driven b_5 effects. A redox effect could appear inconsistent with the observation that b_5 increased substrate oxidation by ferryl−oxo complex (which did not require electron transfer from b_5) but not water formation. However, non-redox b_5 analogues did not enhance 3A4 activity in our membrane-bound conditions, supporting a redox-dependent mechanism. In fact, it can be questioned whether analogues of b_5 could induce the same conformational effects as native b_5. NMR studies revealed that apo-b_5 was only partially folded in the heme binding domain (*60*, *61*) and may incorrectly interact with 3A4. However, this analogue activated 3A4 activity in reconstituted system. A better folding was expected for Zn-b_5, although the metal in this analogue was not coordinated to b_5 His-39 and His-63, due to the zinc d-orbital saturation. Nevertheless, the absence of the effect on 3A4 was also found with cobalt-b_5 which is hexacoordinated. The NMR structure of hexacoordinated Mn-b_5 was recently reported (*62*) and illustrated a quite native structure. It was thus unlikely that impaired complex formation with 3A4 could explain the absence of the effect of Zn- or Co-b_5 analogues in the membrane-bound conditions.

A generally recognized role of reduced b_5 is to act as an electron source for ferrous−dioxygen complex reduction. In such a mechanism, increase in the rate of P450 cycle initiation by substrates (Table 2, Figure 1) was expected to induce increased rates of b_5 reoxidation. Assuming a constant rate of b_5 reduction by CPR, decreasing steady-state levels of reduced b_5 were expected for increasing 3A4-dependent rates of NADPH oxidation. A completely opposite 3A4 behavior was in fact observed, with a positive correlation between the fraction of reduced b_5 and the rate of P450 cycle initiation. Moreover, a large part of the b_5 reduction course following NADPH addition depended on the presence of 3A4 and was ruled by the nature and concentration of the P450 substrate. Complementary rapid kinetic experiments showed that the 3A4-dependent b_5 reduction occurred at a rate fast enough to be significant compared to the average turnover duration. In addition, anaerobic experiments indicated that reduction of b_5 by 3A4 was competitive with the formation of the 3A4-reduced carbon monoxide spectra, likely due to fast electron redistribution between 3A4 and b_5. Finally, comparison in aerobiosis of the b_5 reduction level at the kinetic plateau to its rate of reduction by 3A4 and to the rate of P450-independent b_5 autoxidation strongly suggested that 3A4 also acted as an electron acceptor for b_5. This 3A4 to b_5 electron shuttle was ruled by the presence of substrate and explained the large 3A4 substrate dependence of the b_5 reduction level in steady-state conditions.

P450 ferrous−dioxygen complexes from $P450_{LM4}$ and $P450_{LM2}$ were previously found to efficiently reduce b_5 in single turnover experiments (*26*). Comparison of b_5 reduction by 3A4 in the presence of oxygen and of carbon monoxide was consistent with b_5 reduction in aerobiosis by an early formed 3A4 oxygenated species, likely the ferrous−dioxygen complex. Similarly, the ferrous−dioxygen complex formed by air titration of reduced $P450_{LM2}$ was found to rapidly oxidize reduced b_5 in rapid kinetic experiments with purified enzymes (*26*). Thus the ferrous−dioxygen complex was at the same time a reducing agent when involved in the $Fe^{II}O_2/Fe^{III}$ couple and an oxidizing agent in the $Fe^{II}O_2/Fe^{III}O_2^{2-}$ couple. Our data were consistent with the occurrence of a similar situation with 3A4, and this hypothesis was used as a basis to build the simulation model presented. In such a scheme, no P450-independent electron source for b_5 reduction was required as 3A4 acted both as an electron source and sink. Consistently, introduction of P450-independent sources of b_5 reduction or oxidation has only marginal effects on simulated 3A4 activities and b_5 effects. This indicated that the limited reduction of b_5 observed experimentally (and simulated) in the absence of 3A4 or substrate did not play a significant role in the mechanism and that the 3A4−b_5−CPR system was self-sufficient. Consistently, addition of b_5 reductase and NADH in the experimental system (data not shown) did not change b_5 effects or 3A4 activities. This suggested a major role in the b_5 effect of synchronized b_5 and 3A4 redox cycles as illustrated in the model.

Adjustment of rate constants in the model was relatively raw. The objective was not to determine a unique set of microscopic constants but to show that this model allowed semiquantitative prediction of all tested experimental behaviors. Analysis of the critical kinetic constants enlightens several interesting properties intrinsic to the scheme. Particularly, the ratio between rate constants for the dissociation of b_5 from the ferryl−oxo complex (k_{15}) and substrate oxidation (k_5) was highly critical for b_5 effects. Interestingly, simulated b_5 effects increased for decreasing values of the b_5 dissociation rate constant. This means that a limited b_5 effect was expected for a rapidly exchanging b_5. This phenomenon might explain why the b_5 enhancing effect seemed to be extremely dependent on the b_5 source and why, for example, yeast b_5 was found to be fully inactive toward

3A4 (*42*). This prediction could also explain why b_5 behavior appeared so contradictory in the literature, depending on experimental conditions and the reconstitution system used (*31*). A second prediction of the model was the possibility to simulate or not an effect for redox-inactive b_5, depending on the value of k_{12}. This constant depended on the efficiency of the reductase to give electrons to b_5-bound compared to b_5-free ferrous−dioxygen 3A4, in other words, on the physical overlap of the b_5 binding site with the preferential electron-transfer site for the reduction of this complex by the reductase. Minor structural changes at the level of the b_5 structure, for example, induced by heme removal could modify this overlap and turn on or off the effect of apo-b_5. A similar effect can also occur from a change in the geometry of the complex, for example, membrane-bound versus micelles in reconstituted systems. This might explain the very contradictory results reported in the literature for the b_5 effects on 3A4 and from a more general point of view for the b_5 effects on the different P450s.

In conclusion, the model presented allowed to explain by redox and site overlap effects all known characteristics of 3A4 activation by b_5. Interestingly, some effects frequently interpreted as unknown conformational effects can now be interpreted without need for any b_5 induced conformational change at the 3A4 level (except site overlap exclusions). Moreover, the contradictory observations in the literature can be made compatible within a single model provided modulation of a unique rate constant. Several undocumented effects were predicted and could be experimentally tested in future experiments. On the basis of experimental data and model-based interpretations, 3A4 activation by b_5 mainly relied on inhibition, by b_5 binding, of electron transfer from CPR to the 3A4 ferryl−oxo complex. While this mechanism was consistent with reported 3A4 activation by redox inactive b_5 in the reconstituted system, redox-competent b_5 was strictly required for effects in the membrane-bound natural system. A shift of a single rate constant in the model is sufficient to explain this bimodal and apparently contradictory behavior.

REFERENCES

1. Capdevila, J. H., Zeldin, D., Makita, K., Karara, A., and Falck, J. R. (1995) in *Cytochrome P450: Structure, Mechanism, and Biochemistry* (Ortiz de Montellano, P. R., Ed.) 2nd ed., pp 443−471, Plenum Press, New York.
2. Guengerich, F. P. (1991) *J. Biol. Chem. 266*, 10019−10022.
3. Porter, T. D., and Coon, M. J. (1991) *J. Biol. Chem. 266*, 13469−13472.
4. Guengerich, F. P., Gillam, E. M. J., Martin, M. V., Baba, T., Kim, B. R., Shimada, T., Raney, K. D., and Yun, C. H. (1994) in *Ernst Schering Research Foundation Workshop 13: Assessment of the Use of Single Cytochrome P450 Enzymes in Drug Research*, pp 161−186, Springer-Verlag, Berlin.
5. Brian, W. R., Sari, M. A., Iwasaki, M., Shimada, T., Kaminsky, L. S., and Guengerich, F. P. (1990) *Biochemistry 29*, 11280−11292.
6. Imaoka, S., Imai, Y., Shimada, T., and Funae, Y. (1992) *Biochemistry 31*, 6063−6069.
7. Shet, M. S., Faulkner, K. M., Holmans, P. L., Fisher, C. W., and Estabrook, R. W. (1995) *Arch. Biochem. Biophys. 318*, 314−321.
8. Shet, M. S., Fisher, C. W., Holmans, P. L., and Estabrook, R. W. (1993) *Proc. Natl. Acad. Sci. U.S.A. 90*, 11748−11752.
9. Yamazaki, H., Gillam, E. M., Dong, M. S., Johnson, W. W., Guengerich, F. P., and Shimada, T. (1997) *Arch. Biochem. Biophys. 342*, 329−337.
10. Yamazaki, H., Nakano, M., Imai, Y., Ueng, Y. F., Guengerich, F. P., and Shimada, T. (1996) *Arch. Biochem. Biophys. 325*, 174−182.
11. Yamazaki, H., Ueng, Y. F., Shimada, T., and Guengerich, F. P. (1995) *Biochemistry 34*, 8380−8389.
12. Halvorson, M., Greenway, D., Eberhart, D., Fitzgerald, K., and Parkinson, A. (1990) *Arch. Biochem. Biophys. 277*, 166−180.
13. Gillam, E. M. J., Baba, T., Kim, B. R., Ohmori, S., and Guengerich, F. P. (1993) *Arch. Biochem. Biophys. 305*, 123−131.
14. Strittmatter, P., Spatz, L., Corcoran, D., Rogers, M. J., Setlow, B., and Redline, R. (1974) *Proc. Natl. Acad. Sci. U.S.A. 71*, 4565−4569.
15. Jansson, I., and Schenkman, J. B. (1987) *Drug Metab. Dispos. 15*, 344−348.
16. Vatsis, K. P., Theoharides, A. D., Kupfer, D., and Coon, M. J. (1982) *J. Biol. Chem. 257*, 11221−11229.
17. Pompon, D., Perret, A., Bellamine, A., Laine, R., Gautier, J. C., and Urban, P. (1995) *Toxicol. Lett. 82*−*83*, 815−822.
18. Urban, P., Truan, G., Gautier, J. C., and Pompon, D. (1993) *Biochem. Soc. Trans. 21*, 1028−1034.
19. Bosterling, B., Trudell, J. R., Trevor, A. J., and Bendix, M. (1982) *J. Biol. Chem. 257*, 4375−4380.
20. Canova-Davis, E., and Waskell, L. (1984) *J. Biol. Chem. 259*, 2541−2546.
21. Noshiro, M., Ullrich, V., and Omura, T. (1981) *Eur. J. Biochem. 116*, 521−526.
22. Sugiyama, T., Miki, N., and Yamano, T. (1980) *J. Biochem. (Tokyo) 87*, 1457−1467.
23. Tamburini, P. P., and Schenkman, J. B. (1987) *Proc. Natl. Acad. Sci. U.S.A. 84*, 11−15.
24. Taniguchi, H., Imai, Y., and Sato, R. (1984) *Arch. Biochem. Biophys. 232*, 585−596.
25. Bonfils, C., Balny, C., and Maurel, P. (1981) *J. Biol. Chem. 256*, 9457−9465.
26. Pompon, D., and Coon, M. J. (1984) *J. Biol. Chem. 259*, 15377−15385.
27. Imai, Y., and Sato, R. (1977) *Biochem. Biophys. Res. Commun. 75*, 420−426.
28. Morgan, E. T., and Coon, M. J. (1984) *Drug Metab. Dispos. 12*, 358−364.
29. Sugiyama, T., Miki, N., Miyake, Y., and Yamano, T. (1982) *J. Biochem. (Tokyo) 92*, 1793−1803.
30. Tamburini, P. P., White, R. E., and Schenkman, J. B. (1985) *J. Biol. Chem. 260*, 4007−4015.
31. Yamazaki, H., Johnson, W. W., Ueng, Y. F., Shimada, T., and Guengerich, F. P. (1996) *J. Biol. Chem. 271*, 27438−27444.
32. Lee, C. A., Kost, T. A., and Serabjit-Singh, C. J. (1996) *Methods Enzymol. 272*, 86−95.
33. Gonzalez, F. J., Kimura, S., Tamura, S., and Gelboin, H. V. (1996) *Methods Enzymol. 272*, 93−99.
34. Guengerich, F. P., Gillam, E. M. J., Ohmori, S., Sandhu, P., Brian, W. R., Sari, M. A., and Iwasaki, M. (1993) *Toxicology 82*, 21−37.
35. Aoyama, T., Nagata, K., Yamazoe, Y., Kato, R., Matsunaga, E., Gelboin, H. V., and Gonzalez, F. J. (1990) *Proc. Natl. Acad. Sci. U.S.A. 87*, 5425−5429.
36. Guengerich, F. P., and Johnson, W. W. (1997) *Biochemistry 36*, 14741−14750.
37. Patten, C. J., and Koch, P. (1995) *Arch. Biochem. Biophys. 317*, 504−513.
38. DePierre, J. W., and Ernster, L. (1977) *Annu. Rev. Biochem. 46*, 201−262.
39. DePierre, J. W., and Dallner, G. (1975) *Biochim. Biophys. Acta 415*, 411−472.
40. Estabrook, R. W., Franklin, M. R., Cohen, B., Shigamatzu, A., and Hildebrandt, A. G. (1971) *Metabolism 20*, 187−199.
41. Shephard, E. A., Phillips, I. R., Bayney, R. M., Pike, S. F., and Rabin, B. R. (1983) *Biochem. J. 211*, 333−340.

42. Truan, G., Cullin, C., Reisdorf, P., Urban, P., and Pompon, D. (1993) *Gene 125*, 49−55.
43. Mueller, E. J., Loida, P. J., and Sligar, S. G. (1995) in *Cytochrome P450: Structure, Mechanism, and Biochemistry* (Ortiz de Montellano, P. R., Ed.) 2nd ed., pp 83−124, Plenum Press, New York.
44. Oprian, D. D., Gorsky, L. D., and Coon, M. J. (1983) *J. Biol. Chem. 258*, 8684−8691.
45. Atkins, W. M., and Sligar, S. G. (1988) *Biochemistry 27*, 1610−1616.
46. Atkins, W. M., and Sligar, S. G. (1987) *J. Am. Chem. Soc. 109*, 3754−3760.
47. Gorsky, L. D., Koop, D. R., and Coon, M. J. (1984) *J. Biol. Chem. 259*, 6812−6817.
48. Loev, B., and Snader, K. M. (1965) *J. Org. Chem. 30*, 1914−1916.
49. Peyronneau, M. A., Renaud, J. P., Truan, G., Urban, P., Pompon, D., and Mansuy, D. (1992) *Eur. J. Biochem. 207*, 109−116.
50. Pompon, D., Louerat, B., Bronine, A., and Urban, P. (1996) *Methods Enzymol. 272*, 51−64.
51. Cullin, C., and Pompon, D. (1988) *Gene 65*, 203-217.
52. Strittmatter, P. (1960) *J. Biol. Chem. 235*, 2492−2497.
53. Clark, W. M., Taylor, J. F., Davies, T. H., and Vestling, C. S. (1940) *J. Biol. Chem. 135*, 543.
54. Guengerich, F. P., Muller-Enoch, D., and Blair, I. A. (1986) *Mol. Pharmacol. 30*, 287−295.
55. Guilbault, G. G., Kramer, D. N., and Hackley, E. (1967) *Anal. Chem. 39*, 271−272.
56. Gautier, J. C., Urban, P., Beaune, P., and Pompon, D. (1996) *Chem. Res. Toxicol. 9*, 418−425.
57. Pompon, D. (1987) *Biochemistry 26*, 6429−6435.
58. Sligar, S. G. (1976) *Biochemistry 15*, 5399−5406.
59. Staudt, H., Lichtenberger, F., and Ullrich, V. (1974) *Eur. J. Biochem. 46*, 99−106.
60. Falzone, C. J., Mayer, M. R., Whiteman, E. L., Moore, C. D., and Lecomte, J. T. (1996) *Biochemistry 35*, 6519−6526.
61. Moore, C. D., and Lecomte, J. T. (1993) *Biochemistry 32*, 199−207.
62. Gruenke, L. D., Sun, J., Loehr, T. M., and Waskell, L. (1997) *Biochemistry 36*, 7114−7125.

BI980908Q